

Interplay of slip and twinning in niobium single crystals compressed at 77 K

Roman Gröger,^{a)} Zdeněk Chlup, Tereza Kuběnová, and Ivo Kuběna

Institute of Physics of Materials & CEITEC IPM, Academy of Sciences of the Czech Republic, Brno 61600, Czech Republic

(Received 15 July 2018; accepted 3 October 2018)

High-purity niobium single crystals of five different orientations were compressed at 77 K to 2–4% plastic strain to investigate the mechanisms operative in the initial stage of yielding. The crystals deformed in the direction close to the [001] axis exhibit predominant slip on the high-stressed (101) and a much lower stressed (0 $\bar{1}1$) plane. The expected slip on the ($\bar{1}01$) plane is nearly homogeneously distributed with only a few sharp slip traces corresponding to localized slip. The samples compressed along center-triangle orientations and those close to the [011] – [$\bar{1}11$] edge deform predominantly by twinning on {112}⟨111⟩ systems with some contribution from slip on the ($\bar{1}01$)[$\bar{1}\bar{1}\bar{1}$] system with the highest Schmid factor. A majority of twins exhibit internal contrast due to alternating slip on ($\bar{1}01$) and (0 $\bar{1}1$) planes. No slip traces are observed in the matrix adjacent to the twin, which implies that twin boundaries are impenetrable obstacles for the motion of dislocations.

I. INTRODUCTION

The plastic deformation of crystalline materials results from dislocation glide or mechanical twinning. The choice of a particular deformation mode is to a great extent controlled by crystal symmetry.¹ In particular, body-centered cubic (bcc) metals are expected to deform by dislocation glide on some of their twelve {110}⟨111⟩ systems.² However, a large number of experiments made on Nb single crystals at low temperatures suggest that its mechanism of plastic deformation varies with the character and orientation of the applied load.^{3–20} If the uniaxial load is applied such that the loading axis lies within the [001] – [011] – [$\bar{1}11$] stereographic triangle, different behavior is generally observed for loading directions close to the [001] axis (hereafter referred to as the region I), in the central part of the triangle (region II), and close to the [011] – [$\bar{1}11$] edge of the triangle (region III).

If the load is applied in region I, Nb deforms by pure slip on {110} planes in both tension and compression.¹⁶ Due to the proximity of the [001] axis with 4-fold symmetry, the slip takes place predominantly on ($\bar{1}01$), (101), (0 $\bar{1}1$), and (011) planes, which belong to the slip systems with the highest Schmid factors. The stress–strain curves in tension are often serrated and accompanied by small load drops.¹⁴ Due to small strain inhomogeneity in the initial stage of plastic deformation, the relative contribution of individual slip systems may

differ significantly at different positions on the surface. While Duesbery and Foxall⁹ report on dominant (0 $\bar{1}1$) slip in tension below 150 K, Wasserbäch and Novák¹⁸ show comparable slip on the (0 $\bar{1}1$) and (101) planes in tension at 77 K. Strong slip on the (0 $\bar{1}1$) plane after 3% prestrain at room temperature was also observed by Louchet and Kubin¹³ in crystals deformed in tension at 50 K. However, earlier tests on single crystals of Nb and its dilute alloys often lead to macroscopic slip on planes different from {110}. In particular, a majority of slip traces in the experiments of Reid, Gilbert, and Hahn⁵ made in tension at 77 K correspond to traces of ($\bar{1}\bar{1}2$) and (0 $\bar{1}1$) planes, whereas their samples compressed at 77 K exhibited traces on ($\bar{1}01$) and (101) planes. For Nb + 5 at.% Mo alloys deformed in tension at 77 K, Statham, Veselý, and Christian¹⁰ observed slip on the maximum resolved shear stress (MRSS) plane. However, their compression experiments on the same material and at the same temperature lead to the ($\bar{1}01$) slip.

If the crystal is loaded along a direction in region II, the slip morphology differs markedly for crystals loaded in tension and compression. In tension, Bolton and Taylor¹¹ observed dominant slip on (0 $\bar{1}1$) planes with very little slip on ($\bar{1}01$) and (101) planes. The slip on the (0 $\bar{1}1$) plane was unexpected due to very low Schmid factors of (0 $\bar{1}1$)[111] and (0 $\bar{1}1$)[$\bar{1}\bar{1}\bar{1}$] systems compared to that of the (101)[111] system. The stress–strain curves were often serrated, especially in the initial stage of deformation, but these serrations were replaced by smooth hardening at larger strains.^{11,14} The observation of (0 $\bar{1}1$) anomalous slip is in accordance with experiments of Garrat-Reed and Taylor¹⁶ in tension at 77 K,

^{a)}Address all correspondence to this author.

e-mail: groger@ipm.cz

DOI: 10.1557/jmr.2018.398

where the expected slip on the $(\bar{1}01)$ plane was never observed and the (101) conjugate slip was only observed at large strains (around 10%). Dominant $(0\bar{1}1)$ anomalous slip in tension is also reported by Duesbery and Foxall⁹ below 150 K and by Wasserbäch and Novák¹⁸ at 77 K. Prestraining at room temperature and surface damage by abrasion lead to much finer and more uniformly distributed $(0\bar{1}1)$ traces.¹⁵ Much work has been conducted to expose the relation between interstitial impurities and the anomalous slip. The early experiments of Reid, Gilbert, and Hahn⁵ in tension at 77 K with loading direction in region II show that less pure samples exhibit slip along $(\bar{1}\bar{1}2)$ planes instead of the $(0\bar{1}1)$ anomalous slip. Interstitial impurities thus seem to suppress anomalous slip in Nb.²⁰ Unlike loading in tension, compression in region II leads to preferential twinning. In crystals compressed at 77 K, Boucher and Christian¹² observed primary twinning on $(\bar{2}11)$ and (211) planes and fewer twins on $(\bar{1}21)$ and (121) planes. This twinning was always accompanied by audible clicks and load drops and was suppressed by prestrain. Their conclusions are supported by later studies of Garratt-Reed and Taylor,¹⁴ who also add that testing above 77 K completely suppresses load drops. Furthermore, their more recent experiments show that for some orientations in region II, Nb single crystals deform by a combination of slip and twinning.¹⁶ These conclusions again differ from the studies made on less pure samples, which show either $\{110\}$ slip⁵ or $(\bar{1}01)$ slip with a deviation toward the MRSS plane for orientations closer to region III.¹⁰

The most striking differences between the slip morphology in tension and compression occur if the crystal is loaded in region III. High-purity samples of Garratt-Reed and Taylor¹⁴ loaded in tension at 77 K showed serrated stress-strain curves with large load drops, which diminished on approaching the $[\bar{1}11]$ direction. The slip morphology was characterized by equal amounts of slip on the $(\bar{1}01)$ and $(\bar{1}10)$ planes.¹⁶ Except for the orientations very close to the $[\bar{1}11]$ axis, a few $(0\bar{1}1)$ slip traces were observed as well even though the Schmid factors of both systems containing this slip plane were nearly zero. The tensile experiments of Nagakawa and Meshii¹⁷ at 10–77 K showed large load drops on the stress-strain curves resulting in the formation of $(\bar{1}01)$ shear bands, but no $(0\bar{1}1)$ slip was observed at any temperature. However, less pure samples of Reid, Gilbert, and Hahn⁵ showed $\{110\}$ slip for an orientation close to $[011]$ but “catastrophic slip” on the $(011)[\bar{1}00]$ system (sometimes accompanied by load drops) for loading directions in the vicinity of the $[\bar{1}11]$ axis. The dilute samples of Nb + 5 at.% Mo used by Statham, Veselý, and Christian¹⁰ deformed by slip on the $(\bar{1}01)$ plane. In contrast to tension, the samples of Taylor and Christian⁷ deformed in compression at 77 K exhibited dominant twinning, which was found to be suppressed by prestraining above 90 K.

Similar observations were made by Garratt-Reed and Taylor,^{14,16} who showed that Nb single crystals of high purity compressed at 77 K deformed by profuse twinning on $(\bar{2}11)$ planes and this persisted even in samples prestrained by 2%. The occurrence of twinning was associated with load drops that, however, vanished above 77 K. Interestingly, preferential twinning was observed also in less pure samples of McHargue.²¹ Similar observations were made by Reid, Gilbert, and Hahn⁵ for the $[011]$ loading direction, where twinning was superseded by $\{211\}$ slip for the orientations close to $[\bar{1}11]$. The persistence of deformation twinning even in less pure samples suggests that twinning may be less affected by small amounts of interstitial impurities. However, it does not take place in dilute Nb+5 at.% Mo alloys of Statham, Veselý, and Christian,¹⁰ which deformed by pure slip on the MRSS plane.

It has been known for a long time that the formation of twin embryos in bcc lattices can occur by the dissociation of $1/2\langle 111 \rangle$ screw dislocations into three $1/6\langle 111 \rangle$ partials on parallel $\{112\}$ planes.^{22,23} These fractional dislocations can move with low lattice friction, which may explain why twinning in bcc crystals is nearly temperature-independent. Atomistic simulations due to Vitek,²⁴ Bristowe, Crocker, and Norgett²⁵ and, later, by Ogata, Li, and Yip²⁶ have provided much insight into the structures and energies of multilayer stacking faults forming the twin embryos in these materials. These studies were revisited most recently by Ojha and Sehitoglu,²⁷ whose results show a clear tendency of the bcc metals of the VB group to deform by twinning, whereas those of the VIB group deform predominantly by slip. Molecular dynamics simulations at finite temperatures are generally made at very high strain rates in excess of 10^5 s^{-1} and probe the plastic response under shock loading.^{28–30} Subjected to these extreme environments, Nb as well as most other metals spontaneously twin,³¹ new dislocations may nucleate without the need for dislocation sources, and their glide is not thermally activated.³² First principles studies, while being limited to small number of atoms and fully periodic simulation boxes, have been utilized to obtain information about the shape of the Peierls potential experienced by a moving $1/2[111]$ screw dislocation for virtually all bcc metals.^{33,34}

Most experimental knowledge about the plastic behavior of Nb single crystals under stress has been obtained using samples deformed to plastic strains in excess of 10%,^{3,4,7,10,14,17} which were presumably needed to achieve sufficient contrast of slip traces against the background surface roughness. The surface morphology at these large strains is dominated by intersections between dislocations in noncoplanar slip systems, which mask the mechanism responsible for the initiation of plastic flow. The objective of this paper is to shed light onto understanding of the initial stage of yielding in Nb

single crystals deformed in compression by investigating the changes of surface morphology that take place in the first 2–4% of plastic strain. All experiments discussed in this paper were made at 77 K using small strain rates and loading directions that cover the regions I, II, and III of the stereographic triangle, as defined above. The intensity of observed surface markings is reconciled using the Schmid factors and visibility analyses of elementary surface traces for each system.

II. MATERIALS AND METHODS

The zone-refined and vacuum-treated [110] oriented single crystal of Nb with 99.99% purity was acquired from MaTeck Material-Technologie & Kristalle GmbH (Jülich, Germany). The typical chemical analysis of as-received samples, provided by the manufacturer, gives the following concentration of impurities (in weight ppm): C: 25, O: 15, Al: 3.6, Cr: 1.8, Fe: 3.4, Si: 17.0, Ta: 180. One flat end of this cylindrical specimen was polished mechanically by silicon carbide sandpapers of roughness from grit-220 to 1200. The mechanically hardened surface layer was removed by the standard buffered chemical polishing at ambient temperature in a 1:1:2 solution of HNO_3 : HF : H_3PO_4 . This process resulted in the removal of approx. 100 μm of material from the surface without significant temperature rise. The initial orientation of the crystal was determined by electron backscatter diffraction (EBSD) in the scanning electron microscope TESCAN Lyra 3 XMU FEG/SEMxFIB (TESCAN, Brno, Czech Republic) equipped with the EBSD detector from Oxford Instruments (Abingdon, UK). The orientation analysis was performed using Oxford AZtec software.

The test samples of desired orientations were obtained by electric discharge machining on Sodick SL400Q (Sodick

Europe Ltd., Coventry, UK), and polished mechanically and chemically using the acid solution described above. During the latter step, the samples were kept in a rapidly stirred solution for 30 min to ensure consistent quality of polish on all their sides. The samples of nominal cross sections around $3 \times 3 \text{ mm}$ and lengths 7–8 mm were deformed in compression on Instron 8862 (Norwood, Massachusetts) inside a liquid nitrogen chamber. The uniaxial compression was applied in the position-control mode with the crosshead speed of 30 $\mu\text{m}/\text{min}$, which resulted in the plastic strain rate of $3 \times 10^{-5} \text{ s}^{-1}$. The target plastic strain was chosen deliberately between 2 and 4% to probe the initial stage of plastic deformation. The orientation of each sample before and after deformation was determined using the EBSD analysis, and the results of which are shown in the stereographic triangle in Fig. 1. In the following, the test samples are designated as X–YY, where X identifies the source material and manufacturer and YY distinguishes individual test samples.

Under compression, the loading axis rotates toward the pole that represents the normal of the slip plane that carries most of the plastic strain. For all samples with their initial loading directions close to the center of the stereographic triangle to the $[011] - [\bar{1}11]$ edge, the loading axis rotated toward the $[\bar{2}11]$ axis. This is the normal of the nearest $\{112\}$ plane in the zone of the $[111]$ axis that is sheared in the twinning sense and thus 1/2 $[111]$ screw dislocations may move more easily by macroscopic slip close to this $(\bar{2}11)$ plane than close to the $(\bar{1}\bar{1}2)$ plane sheared in the antitwining sense.⁶ Due to the large load drops for these orientations, one may also anticipate the presence of deformation twinning on $\{112\}$ planes. The prediction of the dominant slip plane for the sample 2-08 loaded in the vicinity of the $[001]$

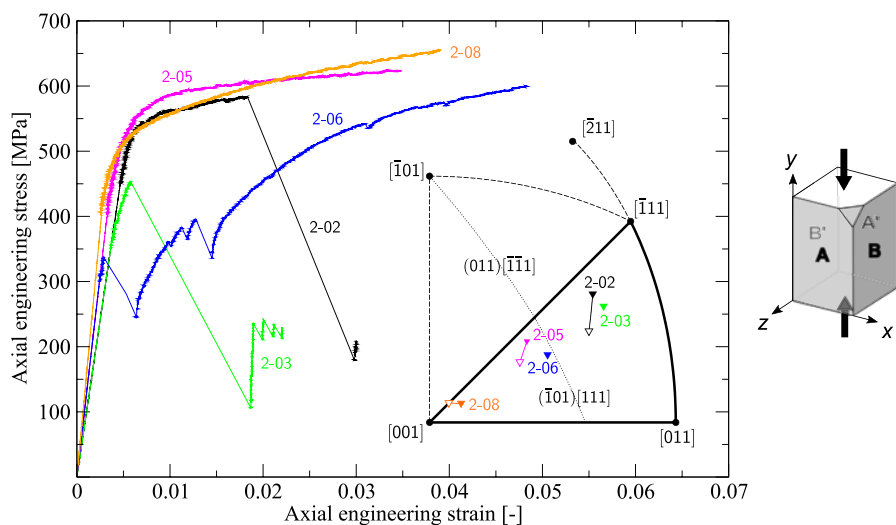


FIG. 1. The stress–strain curves of five Nb single crystals tested in compression corrected for the compliance of the testing machine. The inset shows the orientations of samples before deformation (empty triangles) and after deformation (filled triangles); the orientations of samples 2-03 and 2-06 were only measured after deformation.

axis cannot be made because its negligible lattice rotation is of the same order of magnitude as the error bars inherent in the EBSD analysis.

The stress–strain curves plotted in Fig. 1 show that the mechanism of plastic deformation of high-purity Nb single crystals compressed at 77 K depends strongly on the orientation of the applied load. In particular, the sample 2-08 oriented near the [001] corner and the sample 2-05 near the middle of the [001] – $[\bar{1}11]$ edge deformed smoothly without any load drops or audible clicks. However, even a slight misorientation of the loading axis from 2-05 to 2-06 (i.e., moving closer to the center of the stereographic triangle) and the orientations 2-02 and 2-03 closer to the $[\bar{1}11]$ corner of the triangle resulted in large load drops, in agreement with previous observations.^{5,7,11,17} For the center–triangle orientation (sample 2-06), the load drops are at most 100 MPa and are followed by smooth hardening. However, they are much larger (300–400 MPa) for the samples 2-02 and 2-03, which exhibit an appreciable unloading and subsequent linear-elastic reloading. In the following, we will investigate in detail the surface morphology of two samples whose stress–strain curves in Fig. 1 are representatives of the two classes of behavior discussed above: (i) sample 2-08 whose stress–strain curve shows smooth hardening without any load drop and (ii) the sample 2-02 that exhibits smooth initial hardening followed by a large load drop.

III. SURFACE MORPHOLOGY OF DEFORMED SAMPLES

All figures in this paper are plotted such that the loading direction is parallel to the vertical axis. The surface morphology after deformation was studied on two perpendicular faces of each prismatic specimen, designated A and B in Fig. 1. In some cases, further orientation analysis was made on the opposite faces A' and B'. The orientations of traces of all $\{110\}\langle 111\rangle$ and $\{112\}\langle 111\rangle$ systems were first predicted purely geometrically using the sample orientation measured by EBSD before/after deformation and the orientation of the face under observation. The “visibility” of elementary surface steps arising from the operation of a system α is characterized by the product $|\hat{\nu} \cdot \hat{\mathbf{b}}^\alpha|$, where $\hat{\nu}$ is the unit normal vector of the face under observation (i.e., the viewing direction) and $\hat{\mathbf{b}}^\alpha$ is the unit vector parallel to the slip direction of the system α .

A. Deformation by pure slip

The sample 2-08 was compressed in the direction close to the [001] corner of the stereographic triangle to 3.5% of plastic strain. Theoretical predictions of the slip activity of eight $\{110\}\langle 111\rangle$ systems with the largest Schmid factors and the corresponding visibilities of surface steps on the faces A and B of this sample are

given in Table I. All eight systems have comparable Schmid stresses and are thus expected to contribute nearly equally to the overall plastic strain. Our observations made on the sample 2-08 and the forthcoming description of the mechanism of its plastic deformation hold true also for the sample 2-05 with a similar stress–strain curve albeit a somewhat lower work hardening rate.

The slip morphology in Fig. 2, taken from the faces A and B of this sample after deformation, exhibits significant slip markings along two different planes, which are compared with the orientations of traces of the closest $\{110\}$ planes drawn by lines. The dashed lines were obtained from the orientation of the sample before deformation, whereas the solid lines are the predictions made from the sample orientation after deformation. The most dominant surface markings on the face A, shown in Fig. 2(a), lie within the angular region bounded by the dashed and solid lines for the (101) and (0 $\bar{1}1$) planes. The slip morphology on the face B in Fig. 2(b) reveals that both these systems are operative for this orientation with nearly the same prominence. The relative contributions of these systems were found to vary somewhat with the position on the surface, which suggests some inhomogeneity of strain in the initial stage of plastic deformation. The significant misorientation of the predicted (0 $\bar{1}1$) trace with the closest observed slip trace cannot be attributed to the small lattice rotation of the sample during deformation. A possible explanation of this phenomenon may be a combination of the primary slip on the (0 $\bar{1}1$) plane complemented by the (101) slip at higher stresses. If the latter slip was distributed homogeneously between the traces of (101) planes shown in Fig. 2(b), it would effectively shear the pre-existing (0 $\bar{1}1$) steps and thus change their orientation. The strong contribution of the (0 $\bar{1}1$) slip for this orientation is not unexpected owing to large Schmid factors of the two systems that share this slip plane (see Table I). A very similar morphology was obtained previously by Wasserbäch²⁰ on their sample Nb Z44-77 deformed in tension at 77 K to 4.3% plastic strain.

TABLE I. The eight most highly stressed $\{110\}\langle 111\rangle$ systems determined for the $[\bar{1}118]$ direction, which corresponds to the orientation of the sample 2-08 before deformation (this sample rotates negligibly during the deformation). The next system not shown in the table has the Schmid factor of 0.045.

System (α)	Schmid factor	$ \hat{\nu} \cdot \hat{\mathbf{b}}^\alpha ^A$	$ \hat{\nu} \cdot \hat{\mathbf{b}}^\alpha ^B$
(0 $\bar{1}1$)[$\bar{1}11$]	0.428	0.80	0.17
($\bar{1}01$)[$\bar{1}11$]	0.428	0.81	0.07
($\bar{1}0\bar{1}$)[$\bar{1}11$]	0.426	0.12	0.76
(0 $\bar{1}1$)[1 $\bar{1}\bar{1}$]	0.426	0.12	0.76
(0 $\bar{1}\bar{1}$)[111]	0.383	0.81	0.07
(101)[1 $\bar{1}\bar{1}$]	0.383	0.80	0.17
(10 $\bar{1}$)[$\bar{1}11$]	0.381	0.13	0.85
(011)[$\bar{1}1\bar{1}$]	0.381	0.13	0.85

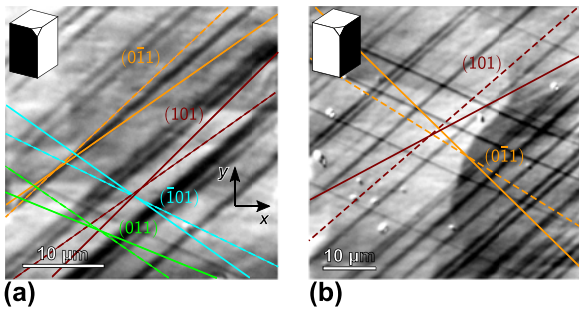


FIG. 2. Slip traces observed on the two perpendicular faces of the sample 2-08 oriented close to the $[001]$ corner of the stereographic triangle: (a) face A and (b) face B. The dashed lines are traces of $\{110\}$ planes determined from the orientation of the sample before deformation, whereas solid lines correspond to the orientation after deformation.

The less visible surface markings in Fig. 2(a) agree well with the traces of $(\bar{1}01)$ and (011) planes and are attributed to the operation of the $(\bar{1}01)[\bar{1}\bar{1}\bar{1}]$ and $(0\bar{1}\bar{1})[\bar{1}\bar{1}\bar{1}]$ systems with the highest Schmid stresses and large visibilities on this face. Other parts of this surface reveal the presence of two sets of mutually misoriented slip traces with nearly the same contrast. They fall into the angular regions of $(\bar{1}01)$ and (011) slip shown in Fig. 2(a), which implies that the two systems above are operative with nearly the same prominence. The distributions of surface traces arising from these systems seem to be rather uniform, as evidenced by a weak roughness parallel to the traces of both planes in the upper right corner of Fig. 2(a).

B. Deformation by a combination of slip and twinning

A very different surface morphology is anticipated for the sample 2-02 oriented closer to the $[011] - [\bar{1}11]$ edge of the stereographic triangle and compressed to 2.3% of plastic strain. The stress-strain curve for this sample, shown in Fig. 1, exhibits smooth initial hardening that was followed by a single large load drop at higher strain accompanied by audible click. To assess the relative activity of slip and twinning systems, we give in Table II the list of the most operative $\{110\}\langle 111\rangle$ and $\{112\}\langle 111\rangle$ systems for this orientation ordered by their Schmid factors. The mechanism of plastic deformation of the samples 2-03 and 2-06 is very similar to the behavior of the sample 2-02 described here.

The surface morphology on the face A of this sample after deformation is shown in Fig. 3(a). It is dominated by two sets of deformation bands that are aligned parallel to the traces of $(\bar{2}11)$ and $(\bar{1}21)$ planes. The EBSD analysis was used to investigate the misorientations of the crystal axes that coincide with the x , y , and z directions in the band and in the surrounding crystal. The maps obtained for the locations marked T1 and T2 are shown next to the

TABLE II. The six most highly stressed $\{110\}\langle 111\rangle$ and $\{112\}\langle 111\rangle$ systems determined for the $[\bar{1}1\ 14\ 24]$ direction, which corresponds to the orientation of the sample 2-02 after deformation. The subscripts T or AT indicate whether a particular $\{112\}$ plane is sheared in the twinning or antitwining sense, respectively. The next $\{110\}\langle 111\rangle$ system not shown in the table has the Schmid factor of 0.125, whereas the next $\{112\}\langle 111\rangle$ system has the Schmid factor of 0.107.

System (α)	Schmid factor	$ \hat{v} \cdot \hat{b}^\alpha ^A$	$ \hat{v} \cdot \hat{b}^\alpha ^B$
$(\bar{1}01)[\bar{1}\bar{1}\bar{1}]$	0.432	0.83	0.18
$(0\bar{1}\bar{1})[\bar{1}\bar{1}\bar{1}]$	0.365	0.77	0.49
$(\bar{1}\bar{1}0)[111]$	0.309	0.83	0.18
$(\bar{1}0\bar{1})[\bar{1}\bar{1}\bar{1}]$	0.291	0.12	0.31
$(\bar{1}10)[11\bar{1}]$	0.240	0.77	0.49
$(0\bar{1}\bar{1})[\bar{1}\bar{1}\bar{1}]$	0.224	0.12	0.31
$(\bar{2}11)[\bar{1}\bar{1}\bar{1}]_T$	0.428	0.83	0.18
$(\bar{1}21)[11\bar{1}]_T$	0.349	0.77	0.49
$(\bar{1}\bar{1}2)[\bar{1}\bar{1}\bar{1}]_{AT}$	0.321	0.83	0.18
$(1\bar{1}2)[1\bar{1}\bar{1}]_{AT}$	0.297	0.12	0.31
$(112)[111]_{AT}$	0.283	0.77	0.49
$(211)[\bar{1}\bar{1}\bar{1}]_T$	0.207	0.12	0.31

micrograph in Fig. 3(a). The maps corresponding to T1 were measured directly on the face A. However, the maps of T2 could not be obtained from the face A due to large surface steps associated with the deformation bands inside this region and thus inconclusive analysis of Kikuchi patterns. Instead, these were obtained from the face A' after repolishing and were mirrored around the vertical axis to correspond to the orientation of the micrograph in Fig. 3(a). In the case of the region T1, the orientation of the blue region corresponding to the x -axis is characterized by the Euler angles $(246, 32, 79)^\circ$, whereas the purple band has Euler angles $(103, 19, 2)^\circ$. The angles between the x , y , and z axes in the two regions were calculated by considering all 24 symmetry operations of the cubic lattice that do not change the handedness of the local coordinate system spanned by these axes. This analysis gives 59° misorientation of the x axes in the two regions, 44° misorientation for the y axes, and 40° for the z axes. A similar analysis made for the region T2 provides the Euler angles $(251, 31, 75)^\circ$ corresponding to the blue region in the map for the x axis, and $(152, 35, 21)^\circ$ for the orange band. The smallest misorientations of axes in these two regions are 55° for the x axes, 27° for the y axes, and 57° for the z axes. These large misorientations of the crystal inside the $\{112\}$ bands with the surrounding matrix provide evidence that both bands in T1 and T2, as well as all parallel surface markings, constitute deformation twins. The two nearly parallel $\{112\}$ traces shown in Fig. 3(a) and corresponding to T1 arise due to twinning on the systems $(\bar{2}11)[\bar{1}\bar{1}\bar{1}]$ and $(\bar{1}21)[11\bar{1}]$, both sheared in the twinning sense. The less numerous twins observed in T2 are close to the traces of $(\bar{1}\bar{1}2)$ and (112) planes, which would be produced by the systems $(\bar{1}\bar{1}2)[\bar{1}\bar{1}\bar{1}]$ and $(112)[11\bar{1}]$, respectively. According to Table I, both these systems

have high visibility on this face and are sheared in the antitwinning sense. It should be emphasized that these traces constitute only a small portion of all twins in this sample. Because twinning in bcc lattices is governed by the motion of screw dislocations with fractional Burgers vectors,²³ their glide on the planes sheared in the antitwinning sense is possible, although its probability at 77 K drops significantly compared to room temperature.⁶

The surface morphology of the face B of this sample is shown in Fig. 3(b). One set of surface markings corresponds to slip on the $(\bar{1}01)[\bar{1}\bar{1}\bar{1}]$ system with the highest Schmid stress but low visibility according to Table II. This observation implies high activity of this system because many dislocations had to move on the same $(\bar{1}01)$ plane to produce noticeable surface traces. The character of the band that passes through the region T3 in Fig. 3(b) was determined by the EBSD analysis, whose results are shown as orientational maps for the x , y , and z axes next to the micrograph. The blue/purple region in the map for the z axis is characterized by the Euler angles $(231, 42, 49)^\circ$, whereas the orange band has Euler angles $(124, 17, 6)^\circ$. The smallest misorientations of these axes in the band relative to the matrix are 59° for the x axis,

25° for the y axis, and 54° for the z axis. These large misorientations prove that the band shown in T3, as well as all parallel surface markings, are deformation twins. These twin needles are long and nucleate predominantly in the vicinity of $(\bar{1}01)[\bar{1}\bar{1}\bar{1}]$ slip traces, which were presumably generated during the smooth hardening preceding the large load drop in Fig. 1. The strain at twin tips is often accommodated by emissary slip on $\{110\}$ planes and, reciprocally, slip traces are observed to emanate from twin boundaries, as considered previously by Mahajan.²² However, these twins are not aligned precisely with the trace of the closest $\{112\}$ plane. The origin of this misalignment may be similar to that discussed earlier with reference to $(0\bar{1}1)$ traces in Fig. 2(b), i.e., shearing the twin away from its initial orientation by homogeneous slip on $(\bar{1}01)$ planes.

The orientational maps for region T4 were not measured because these bands appear predominantly on the face B of the sample and are much less prominent on the opposite face B', from which the EBSD analysis was made after repolishing. A closer inspection of the face B, a part of which is shown in Fig. 3(b), reveals that most of these nearly horizontal bands are associated with the intersections between the twin T3 and the $(\bar{1}01)[\bar{1}\bar{1}\bar{1}]$ slip band. It will be shown in the forthcoming that the internal structure of the band in T4 is similar to those in T1, T2, and T3, which provides circumstantial evidence that also the T4 band constitutes a deformation twin.

IV. STRUCTURE OF DEFORMATION TWINS

The electron micrographs of the four twinned regions in Figs. 3(a) and 3(b) are shown in Fig. 4. The twins T1 and T3 in Figs. 4(a) and 4(c), respectively, form on $\{112\}$ planes that are sheared in the twinning sense. They both exhibit interesting contrast represented by surface traces in two different directions. These structures were observed previously by McHargue,²¹ who attributed them to $\{110\}$ slip within the twins. The slip traces are clearly observed only inside the twin and do not traverse into the surrounding matrix, which suggests that the twin was created first, followed by the nucleation of internal slip within the twin, i.e., compressed along a different direction than the matrix. Interestingly, the lines within the twin match very well with the traces of $(\bar{1}01)$ and $(0\bar{1}1)$ planes obtained for the orientation of the twin. Following the twin formation, the crystal inside the twin is compressed along the $[\bar{3} 10 40]$ direction for which the Schmid factors of the systems $(\bar{1}01)[\bar{1}\bar{1}\bar{1}]$, $(0\bar{1}1)[\bar{1}\bar{1}\bar{1}]$, and $(\bar{1}10)[\bar{1}\bar{1}\bar{1}]$ are 0.483, 0.337, and 0.146, respectively (the slip trace visibility is 0.73 for all three systems). These results suggest that $1/2[111]$ screw dislocations preferentially cross-slip between the $(\bar{1}01)$ and $(0\bar{1}1)$ planes, in agreement with Fig. 4(a). The $(0\bar{1}1)[111]$ system has only the fifth largest Schmid factor for the

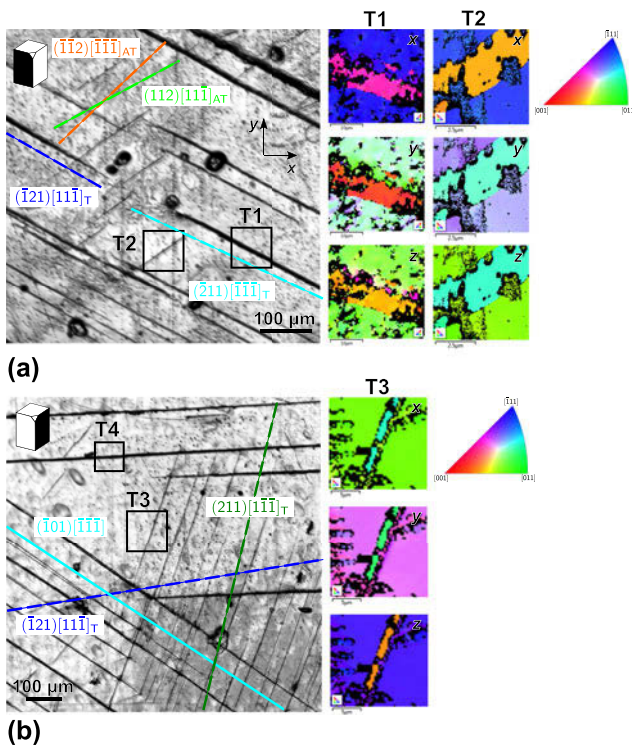


FIG. 3. Surface morphology of the sample 2-02 after deformation: (a) face A and (b) face B. The color figures show the orientation maps for the x , y , and z axes shown in (a). The subscript T (or AT) indicates whether the corresponding $\{112\}$ plane is sheared in the twinning (or antitwinning) sense. The black regions in the orientation maps are parts of the surface, where the analysis of Kikuchi patterns was inconclusive.

orientation of the twin and thus its operation results in anomalous slip. The observed traces cannot be composed using two $\{110\}$ planes corresponding to other $1/2\langle 111 \rangle$ screw dislocations. Apart from the $\{110\}$ slip within the twin, some twins display also sharp contrast along a line inside the twin that is parallel to the twin-matrix interface, as shown in Fig. 4(a). The EBSD analysis of the T1 region in Fig. 3(a) proves that the whole twin has the same orientation and thus the structure does not represent a symmetrically related double-twin. Moreover, the $\{110\}$ slip traces observed in the two parts of the twin seem to be reflected from this central line, which suggests that the structure in Fig. 4(a) is a composite twin formed by merging two closely spaced twins with the same twin boundary and the direction of twinning.

This analysis was made also for the twin in the region T3 in Fig. 3(b) as shown in Fig. 4(c). During further compression following the twin formation, the crystal inside the twin is compressed along the $[4\ 15\ 19]$ direction. The Schmid factors of the $(\bar{1}01)[\bar{1}\bar{1}\bar{1}]$, $(0\bar{1}1)[\bar{1}\bar{1}\bar{1}]$, and $(\bar{1}10)[\bar{1}\bar{1}\bar{1}]$ systems are 0.468, 0.081, and 0.387, respectively, with the same visibility of 0.70. The nearly vertical lines inside the twin are close to the trace of the $(0\bar{1}1)$ plane in the twin, which is interesting owing to very low Schmid factor of this system. In principle, these traces can also originate from the

operation of the $(0\bar{1}1)[\bar{1}\bar{1}\bar{1}]$ system with a different slip direction, but its Schmid factor is equally low (0.103) and its visibility is even lower (0.40) compared to the system above. The interior of the twin shown in Fig. 4(c) does not show any other trace besides $(0\bar{1}1)$ which implies primary slip of $1/2[111]$ and/or $1/2[\bar{1}\bar{1}\bar{1}]$ screw dislocations on this plane.

The nearly horizontal band inside T4 in Fig. 3(b), shown in detail in Fig. 4(d), has a very similar zig-zag contrast to those in T1 and T3 in Figs. 4(a) and 4(c), respectively. This suggests that T4 is also a deformation twin, although we were not able to determine the orientation of this band from the face B' after repolishing due to their sparse appearance on this face. This twin forms close to a $\{112\}$ plane that is sheared in the twinning sense. Its interior exhibits clear traces along two planes, which are again believed to be of the $\{110\}$ type.

The twin T2 shown in Fig. 4(b), which forms on the $\{112\}$ plane sheared in the antitwining sense, does not contain any internal structure. This observation suggests that the slip within this twin is either absent completely or it is distributed homogeneously with the differences in heights of the neighboring slip traces being below the resolution of SEM. No contrast was also obtained by atomic force microscopy. These results provide strong evidence that the observed slip within twins in Nb occurs

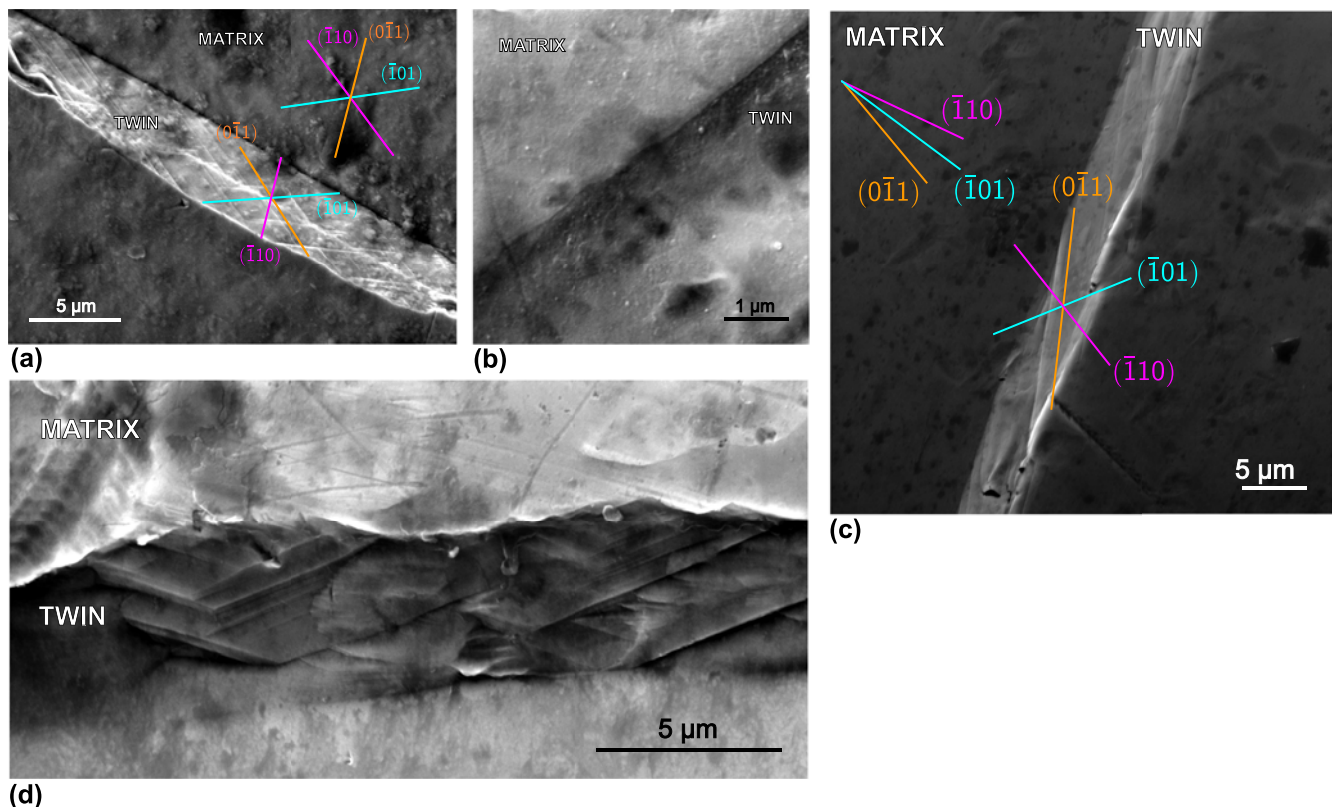


FIG. 4. Internal structures of twins in the sample 2-02 with superimposed predictions of slip traces determined for the orientation of the matrix and the twin. The electron micrographs show the twinned regions in Fig. 3 marked (a) T1, (b) T2, (c) T3, and (d) T4.

more readily in the twins formed on the $\{112\}$ planes sheared in the twinning sense.

V. DISCUSSION

The stress–strain curves in Fig. 1 and the observations made previously in this paper provide ample evidence that Nb single crystals compressed at 77 K deform initially by three different mechanisms: predominant twinning (sample 2-03), slip followed by twinning (sample 2-02), or twinning followed by slip (sample 2-06). The following slip mechanisms may be operative in samples that display significant deformation twinning: (i) the migration of twin boundary dislocations that leads to twin growth and (ii) the glide of $1/2\langle 111 \rangle$ screw dislocations within the twin that leads to the pattern shown in Figs. 4(a), 4(c), and 4(d). The mechanism (i) has nearly zero activation enthalpy arising from small Burgers vectors of twinning dislocations, which results in their easy glide. The motion of twinning dislocations along parallel twin boundaries does not result in strain hardening. On the other hand, the motion of $1/2\langle 111 \rangle$ screw dislocations in the mechanism (ii) requires significant activation enthalpy as well as the energy needed for the cross-slip of these dislocations at the twin boundary.

The presence of slip traces inside twins in Fig. 4 and the lack of hardening in the stress–strain curve of the sample 2-02 in Fig. 1 suggest that the zig-zag slip pattern within the twins arises due to the motion of parallel dislocations with easy cross-slip at the twin boundary due to internal strains. Further evolution of these twins may proceed by twin thickening and/or by the glide of dislocations inside the twins. Two different scenarios can be distinguished here according to the relative rates of these two events. In the extreme case when twin thickening is negligible, screw dislocations moving inside the twin produce overlapping slip traces, resulting in a high-contrast zig-zag slip pattern with segments along both $\{110\}$ planes. On the other hand, if twin thickening proceeds rapidly, the dislocations inside the twin reflect from the twin boundary at different positions, which would lead to nonoverlapping slip traces and a spatially homogeneous slip. From Fig. 4, one observes that a situation similar to the first scenario takes place if the twin forms on the $\{112\}$ plane sheared in the twinning sense. This implies that whenever a twin forms on these planes, the internal slip proceeds more rapidly than twin thickening, which results in the observed zig-zag slip pattern inside these twins.

The observation of preferential twinning under compression for most loading directions within the standard stereographic triangle is not specific only to Nb. We have recently made similar experiments on vanadium single crystals compressed at 77 K, which were observed to deform by pure twinning in the 1–2% of plastic strain

for any orientation of the applied load.³⁵ However, a completely different behavior was observed for our tantalum single crystals compressed at 77 K, which deformed by slip for all loading directions considered. Similarly, no twin formation was observed in molybdenum³⁶ and tungsten compressed at room temperature, which is a low homologous temperature for both metals owing to their high melting temperatures. These observations agree with the trends in twinning stresses determined by Ojha and Sehitoglu²⁷ using atomistic simulations, which increase in the sequence V, Nb, Ta, Mo, and W. The mechanism of plastic deformation of Nb single crystals in compression thus seems to be intermediate between that governing the plastic flow of V (pure twinning) and Ta (pure slip).

VI. CONCLUSIONS

We have made a series of low-temperature experiments on high purity Nb single crystals at 77 K to elucidate the mechanism that is operative in the first 2–4% of plastic strain. The stress–strain curve for the sample compressed in the direction close to the $[001]$ axis and one center–triangle orientation are smooth and suggest deformation by pure slip. The internal strain generated by the applied load is relieved by forming surface traces predominantly on the $(0\bar{1}1)$ and (101) planes. Interestingly, the expected $(\bar{1}01)$ slip seems to be distributed homogeneously with only a few detectable traces corresponding to localized slip.

By contrast, another sample with the center-triangle orientation as well as all samples with orientations near the $[011] - [\bar{1}11]$ edge of the stereographic triangle deform predominantly by twinning on $\{112\}$ planes, which is accompanied by load drops and audible clicks. Depending on the direction of the applied load, these load drops are often preceded or followed by smooth hardening representative of slip. Most of the detectable surface markings are aligned with the traces of $(\bar{1}01)$ planes and arise from the operation of the $(\bar{1}01)[\bar{1}\bar{1}\bar{1}]$ system with the highest Schmid factor. However, a majority of deformation bands are represented by twins on $\{112\}$ planes sheared in the twinning sense, which exhibit internal contrast composed of zig-zag slip traces along $(\bar{1}01)$ and $(0\bar{1}1)$ planes. Detailed electron microscopy studies of the structure of these twins provide evidence that the plastic deformation of Nb single crystals compressed along the directions from the center of the stereographic triangle to the $[011] - [\bar{1}11]$ edge occurs predominantly by twinning with the subsequent slip within the twins nucleated from the twin–matrix boundary at the side of the twin. These traces are localized in the interior of the twin without any detectable traces crossing into the matrix, which suggests that twin boundaries act as strong obstacles for moving dislocations. Instead, the

$1/2[111]$ screw dislocations moving on $(\bar{1}01)$ planes within the twin cross-slip upon reaching the twin boundary into the $(0\bar{1}1)$ plane and continue to move on this plane until they reach the opposite twin boundary, where they cross-slip back into the $(\bar{1}01)$ plane. These zig-zag slip traces were observed only in twins that form on the $\{112\}$ planes sheared in the twinning sense. Nevertheless, a few twin needles were also found on the $\{112\}$ planes sheared in the antitwinning sense, but these do not exhibit any internal contrast even in high-magnification electron micrographs.

The observation of preferential twinning in Nb at low temperatures implies that the link between the degree of crystal symmetry (i.e., the number of available slip systems) and the mechanism of plastic deformation does not hold as firmly even at low strain rates. The abundance of slip within the twins formed on $\{112\}$ planes sheared in the twinning sense and their nonexistence in the twins on $\{112\}$ planes sheared in the antitwinning sense agrees qualitatively with the work of Foxall, Duesbery, and Hirsch⁶ who showed that the likeliness of “slip in the antitwinning sense” drops significantly from room temperature to 77 K. The observations of both slip and twinning in a crystal of high purity used in this work does not support the argument of Duesbery⁴ and Bolton and Taylor¹¹ that twinning in these crystals may be due to the removal of mobile dislocations by annealing. Finally, the observation of twinning as the dominant mechanism governing the plastic deformation of Nb single crystals compressed at low temperatures for most orientations of the applied load challenges the developments of theoretical models of yielding, which assume that the plastic deformation of all bcc metals is controlled by slip on $\{110\}\langle 111\rangle$ systems.

ACKNOWLEDGMENTS

The authors acknowledge helpful discussions on the anomalous slip with Vaclav Vitek. This research was made possible due to financial support from the Czech Science Foundation, Grant No. 16-13797S. It has been carried out under the project CEITEC 2020 (LQ1601) with financial support from the Ministry of Education, Youth and Sports of the Czech Republic under the National Sustainability Programme II.

REFERENCES

1. E. Schmid and W. Boas: *Plasticity of Crystals with Special Reference to Metals* (F.A. Hughes & Co., London, 1950).
2. R. Maddin and N.K. Chen: Geometrical aspects of the plastic deformation of metal single crystals. *Prog. Met. Phys.* **5**, 53 (1954).
3. E. Votava: Eine neue Methode zur Herstellung verformungsfreier Einkristall-Zugproben hochschmelzender Metalle und einige Ergebnisse über die plastische Deformation von Niob-Einkristallen. *Phys. Status Solidi A* **5**, 421 (1964).
4. M.S. Duesbery, R.A. Foxall, and P.B. Hirsch: The plasticity of pure niobium crystals. *J. Phys. Colloq.* **27**, 193 (1966).
5. C.N. Reid, A. Gilbert, and G.T. Hahn: Twinning, slip and catastrophic flow in niobium. *Trans. Metall. Soc. AIME* **236**, 1024 (1966).
6. R.A. Foxall, M.S. Duesbery, and P.B. Hirsch: The deformation of niobium single crystals. *Can. J. Phys.* **45**, 607 (1967).
7. G. Taylor and J.W. Christian: Experiments on the deformation of niobium single crystals. I. Stress versus strain curves and slip systems in compression and tension. *Philos. Mag.* **15**, 873 (1967).
8. G. Taylor and J.W. Christian: Experiments on the deformation of niobium single crystals. II. Electron microscope study of dislocation structures. *Philos. Mag. A* **15**, 893 (1967).
9. M.S. Duesbery and R.A. Foxall: A detailed study of deformation of high-purity niobium single crystals. *Philos. Mag.* **20**, 719 (1969).
10. C.D. Statham, D. Veselý, and J.W. Christian: Slip in single crystals of niobium-molybdenum alloys deformed in compression. *Acta Metall.* **18**, 1243 (1970).
11. C.J. Bolton and G. Taylor: Anomalous slip in high-purity niobium single crystals deformed at 77 K in tension. *Philos. Mag.* **26**, 1359 (1972).
12. N.A. Boucher and J.W. Christian: The influence of pre-strain on deformation twinning in niobium single crystals. *Acta Metall.* **20**, 581 (1972).
13. F. Louchet and L.P. Kubin: Dislocation substructures in the anomalous slip plane of single crystal niobium strained at 50 K. *Acta Metall.* **23**, 17 (1975).
14. A.J. Garratt-Reed and G. Taylor: Stress-strain curves for niobium crystals deformed at temperatures below ambient. *Philos. Mag.* **33**, 577 (1976).
15. R.E. Reed and R.J. Arsenault: Further observations of anomalous slip in niobium single crystals. *Scr. Metall.* **10**, 1003 (1976).
16. A.J. Garratt-Reed and G. Taylor: Optical and electron microscopy of niobium crystals deformed below room temperature. *Philos. Mag. A* **39**, 597 (1979).
17. J. Nagakawa and M. Meshii: The deformation of niobium single crystals at temperatures between 77 and 4.2 K. *Philos. Mag. A* **44**, 1165 (1981).
18. W. Wasserbäch and V. Novák: Optical investigation of anomalous slip-line patterns in high purity niobium and tantalum single crystals after tensile deformation at 77 K. *Mater. Sci. Eng.* **73**, 197 (1985).
19. G. Taylor and M. Saka: Some observations on slip in niobium and Nb-Ti alloy deformed in situ in a HVEM. *Philos. Mag. A* **64**, 1345 (1991).
20. W. Wasserbäch: Anomalous slip in high-purity niobium and tantalum single crystals. *Phys. Status Solidi A* **147**, 417 (1995).
21. C.J. McHargue: Twinning in columbium. *Trans. Metall. Soc. AIME* **224**, 334 (1962).
22. S. Mahajan: Accommodation at deformation twins in bcc crystals. *Metall. Trans. A* **12**, 379 (1981).
23. A.W. Sleeswyk: $1/2\langle 111\rangle$ screw dislocations and the nucleation of $\{112\}\langle 111\rangle$ twins in the b.c.c. lattice. *Philos. Mag. A* **8**, 1467 (1963).
24. V. Vitek: Multilayer stacking faults and twins on $\{211\}$ planes in b.c.c. metals. *Scr. Metall.* **4**, 725 (1970).
25. P.D. Bristowe, A.G. Crocker, and M.J. Norgett: The structure of twin boundaries in body-centred cubic metals. *J. Phys. F: Met. Phys.* **4**, 1859 (1974).
26. S. Ogata, J. Li, and S. Yip: Energy landscape of deformation twinning in bcc and fcc metals. *Phys. Rev. B* **71**, 224102 (2005).
27. A. Ojha and H. Sehitoglu: Twinning stress prediction in bcc metals and alloys. *Philos. Mag. Lett.* **94**, 647 (2014).

28. J. Marian, W. Cai, and V.V. Bulatov: Dynamic transitions from smooth to rough to twinning in dislocation motion. *Nature Mater* **3**, 158 (2004).
29. L.A. Zepeda-Ruiz, A. Stukowski, T. Ooppelstrup, and V.V. Bulatov: Probing the limits of metal plasticity with molecular dynamics simulations. *Nature* **550**, 492 (2017).
30. C.Q. Chen, J.N. Florando, M. Kumar, K.T. Ramesh, and K.J. Hemker: Incipient deformation twinning in dynamically sheared bcc tantalum. *Acta Mater.* **69**, 114 (2014).
31. R.F. Zhang, J. Wang, I.J. Beyerlein, and T.C. Germann: Twinning in bcc metals under shock loading: A challenge to empirical potentials. *Philos. Mag. Lett.* **91**, 731 (2011).
32. D.L. Preston, D.L. Tonks, and D.C. Wallace: Model of plastic deformation for extreme loading conditions. *J. Appl. Phys.* **93**, 211 (2003).
33. L. Ventelon, F. Willaime, E. Clouet, and D. Rodney: Ab initio investigation of the Peierls potential of screw dislocations in bcc Fe and W. *Acta Mater.* **61**, 3973 (2013).
34. L. Dezerald, L. Ventelon, E. Clouet, C. Denoual, D. Rodney, and F. Willaime: Ab initio modeling of the two-dimensional energy landscape of screw dislocations in bcc transition metals. *Phys. Rev. B* **89**, 024104 (2014).
35. R. Gröger, Z. Chlup, T. Kuběnová, and I. Kuběna: Deformation twinning in vanadium single crystals tested in compression at 77 K. *Mater. Sci. Eng., A* **737**, 413 (2018).
36. R. Gröger, Z. Chlup, I. Kuběna, and T. Kruml: Slip activity in molybdenum single crystals compressed at 77 K. *Philos. Mag.* **98**, 2749 (2018).